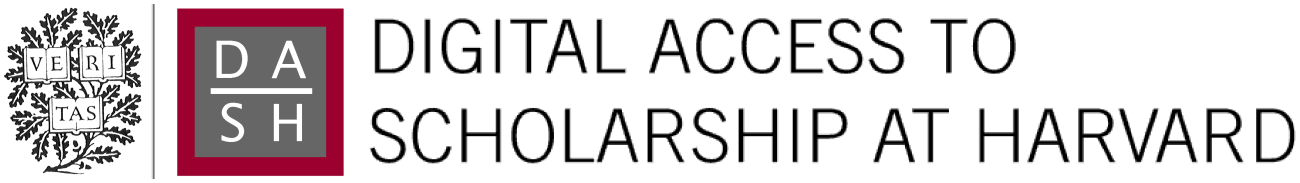

Factors Driving Mercury Variability in the Arctic Atmosphere and Ocean over the Past 30 Years

Factors driving mercury variability in the Arctic atmosphere and ocean over the past 30 years

Jenny A. Fisher,[1] Daniel J. Jacob,[2,3] Anne L. Soerensen,[2,4] Helen M. Amos,[3] Elizabeth S. Corbitt,[3] David G. Streets,[5] Qiaoqiao Wang,[2] Robert M. Yantosca,[2] and Elsie M. Sunderland[2,4]

Received 15 July 2013; revised 2 October 2013; accepted 12 November 2013; published 3 December 2013.

[1] Long-term observations at Arctic sites (Alert and Zeppelin) show large interannual variability (IAV) in atmospheric mercury (Hg), implying a strong sensitivity of Hg to environmental factors and potentially to climate change. We use the GEOS-Chem global biogeochemical Hg model to interpret these observations and identify the principal drivers of spring and summer IAV in the Arctic atmosphere and surface ocean from 1979–2008. The model has moderate skill in simulating the observed atmospheric IAV at the two sites ($r \sim 0.4$) and successfully reproduces a long-term shift at Alert in the timing of the spring minimum from May to April ($r = 0.7$). Principal component analysis indicates that much of the IAV in the model can be explained by a single climate mode with high temperatures, low sea ice fraction, low cloudiness, and shallow boundary layer. This mode drives decreased bromine-driven deposition in spring and increased ocean evasion in summer. In the Arctic surface ocean, we find that the IAV for modeled total Hg is dominated by the meltwater flux of Hg previously deposited to sea ice, which is largest in years with high solar radiation (clear skies) and cold spring air temperature. Climate change in the Arctic is projected to result in increased cloudiness and strong warming in spring, which may thus lead to decreased Hg inputs to the Arctic Ocean. The effect of climate change on Hg discharges from Arctic rivers remains a major source of uncertainty.

Citation: Fisher, J. A., D. J. Jacob, A. L. Soerensen, H. M. Amos, E. S. Corbitt, D. G. Streets, Q. Wang, R. M. Yantosca, and E. M. Sunderland (2013), Factors driving mercury variability in the Arctic atmosphere and ocean over the past 30 years, *Global Biogeochem. Cycles*, *27*, 1226–1235, doi:10.1002/2013GB004689.

1. Introduction

[2] Inputs of inorganic mercury (Hg) to the Arctic Ocean and subsequent methylation and bioaccumulation into marine food webs are major concerns for northern communities who rely on large quantities of fish and marine mammals as part of their traditional diets [*Stow et al*., 2011]. Despite increases in global anthropogenic emissions over the past several decades [*Streets et al*., 2011], Arctic atmospheric Hg levels have decreased or remained constant [*Cole and Steffen*, 2010; *Cole et al*., 2013]. At the same time, both increasing and decreasing trends have been observed in Arctic marine life [*Rigét et al*., 2011], and little is known about seawater Hg concentrations over this period. Major gaps remain in our understanding of the drivers of Hg inputs to the Arctic Ocean and the net effect of climate change on atmospheric and oceanic Hg [*Stern et al*., 2012]. Here we use a global biogeochemical Hg model (GEOS-Chem), combined with long-term atmospheric observations from Arctic sites, to investigate the factors controlling Hg concentrations in the Arctic environment and the impacts of changing emissions and climate over the past 30 years.

[3] Mercury is released to the atmosphere from natural and anthropogenic sources as elemental Hg^0 and divalent Hg^{II}. While Hg^{II} is highly water soluble and rapidly removed by deposition, Hg^0 has an atmospheric lifetime of 6–12 months against oxidation and deposition [*Slemr et al*., 1985; *Corbitt et al*., 2011], allowing efficient transport from midlatitude source regions to the Arctic [*Durnford et al*., 2010]. Over the past 30 years, anthropogenic Hg emissions to the atmosphere have shifted dramatically, with decreasing emissions from Europe, Russia, and North America offset by increases from Asia [*Wilson et al*., 2010; *Streets et al*., 2011].

[4] Episodic Hg^0 depletion from the atmosphere is regularly observed in the Arctic boundary layer during springtime due to oxidation by bromine (Br) radicals released photochemically

Additional supporting information may be found in the online version of this article.

[1]School of Chemistry, University of Wollongong, Wollongong, New South Wales, Australia.
[2]School of Engineering and Applied Sciences, Harvard University, Cambridge, Massachusetts, USA.
[3]Department of Earth and Planetary Sciences, Harvard University, Cambridge, Massachusetts, USA.
[4]Department of Environmental Health, Harvard School of Public Health, Boston, Massachusetts, USA.
[5]Decision and Information Sciences Division, Argonne National Laboratory, Argonne, Illinois, USA.

Corresponding author: J. A. Fisher, School of Chemistry, University of Wollongong, Northfields Ave., Wollongong, NSW 2522, Australia. (jennyf@uow.edu.au)

0886-6236/13/10.1002/2013GB004689

from sea salt deposited on snow and ice [*Simpson et al*., 2007b; *Pratt et al*., 2013]. These atmospheric mercury depletion events (AMDEs) increase Hg deposition [*Ariya et al*., 2004; *Steffen et al*., 2008]. Because the Arctic Ocean remains ice covered throughout the spring, Hg deposited during AMDEs is typically not added directly to the ocean. About 80% of the Hg deposited to snow-covered sea ice during AMDEs is reemitted to the atmosphere within days [*Munthe et al*., 2011]. The remainder stays in surface snow and can eventually enter the ocean upon snowmelt [*Durnford and Dastoor*, 2011].

[5] Mercury also enters the Arctic Ocean through inputs from circumpolar rivers [*Coquery et al*., 1995; *Leitch et al*., 2007; *Graydon et al*., 2009; *Emmerton et al*., 2013] and from erosion of Hg-enriched coastal sediments [*Leitch*, 2006; *Outridge et al*., 2008]. *Fisher et al*. [2012] suggested that these sources may currently be the dominant input of Hg to the Arctic Ocean. The riverine flux peaks in early summer, following breakup and melt of sea ice [*Leitch et al*., 2007; *Graydon et al*., 2009; *Emmerton et al*., 2013]. Observations show elevated oceanic Hg near Arctic river mouths [*Andersson et al*., 2008; *Wang et al*., 2012], with subsequent evasion sufficient to drive local maxima in atmospheric Hg concentrations [*Sommar et al*., 2010].

[6] Biogeochemical Hg cycling in the Arctic is expected to be extremely sensitive to the rapid climate change that has taken place in the region in recent decades [*Macdonald et al*., 2005; *Stern et al*., 2012]. Arctic surface air temperatures have been increasing at a rate nearly 2 times the global average [*Bekryaev et al*., 2010; *Screen and Simmonds*, 2010; *Bintanja et al*., 2011]. Sea ice thickness has decreased by a factor of 2 [*Kwok and Rothrock*, 2009], and annual mean sea ice extent has decreased by 5–10% per decade in most Arctic regions [*Parkinson and Cavalieri*, 2008; *Cavalieri and Parkinson*, 2012]. Over land, permafrost extent has also declined, and the active layer depth of seasonal permafrost thaw has increased [*Zhang et al*., 2005]. This has been accompanied by a steady rise since 1980 in annual freshwater discharge from circumpolar rivers to the Arctic Ocean [*Shiklomanov and Lammers*, 2009].

[7] The effects of changing climate on Hg cycling in the Arctic are multidirectional and complex [*Stern et al*., 2012]. Rising air temperatures drive changes in atmospheric kinetics [*Goodsite et al*., 2004] and decreases in AMDE intensity that could decrease springtime Hg deposition to the ocean [*Piot and von Glasow*, 2008; *Pöhler et al*., 2010]. However, shifts in sea ice regimes from multiyear to first year ice could alternately intensify AMDEs, increasing deposition [*Simpson et al*., 2007a]. Higher temperatures and increased open water area are both expected to increase oceanic Hg evasion, due in part to increased UVB radiation from Arctic ozone depletion and enhanced photochemical Hg reduction [*O'Driscoll et al*., 2006; *Bais et al*., 2011]. Increased productivity in previously ice-covered surface waters [*Arrigo and van Dijken*, 2011] will likely increase particle-associated Hg removal to the subsurface ocean. Mercury inputs to the ocean from the terrestrial system may be affected by increased mobilization from permafrost in some watersheds [*Klaminder et al*., 2008; *Rydberg et al*., 2010] but decreased mobilization in others [*O'Donnell et al*., 2012], along with increased coastal erosion from autumn storms during longer open water seasons [*Atkinson*, 2005; *Lantuit et al*., 2012].

[8] Atmospheric observations at high Arctic stations have been used to evaluate recent changes in Arctic Hg cycling [*Steffen et al*., 2005; *Cole and Steffen*, 2010; *Berg et al*., 2013; *Cole et al*., 2013]. While atmospheric Hg^0 at northern midlatitudes decreased from 2000 to 2009 at a rate of roughly −2% per year, the decrease was only −0.9% per year at Alert in the Canadian Archipelago, and no trend was observed at Zeppelin station on Svalbard [*Berg et al*., 2013; *Cole et al*., 2013]. The particularly long Hg record from Alert (1995 to present) shows a change in peak timing of AMDEs from May in the late 1990s to April in the mid-2000s [*Cole and Steffen*, 2010]. Observations at Alert also show large interannual variability (IAV), particularly in spring [*Steffen et al*., 2005; *Cole and Steffen*, 2010]. These features suggest a large sensitivity of Hg to changes in Arctic climate. However, previous attempts to explain the observed Hg IAV at Alert and Zeppelin with regional meteorological drivers showed no significant correlations apart from air temperature [*Berg et al*., 2013], which only accounted for 16% of Hg variability [*Cole and Steffen*, 2010].

[9] In this work, we use the GEOS-Chem biogeochemical Hg model to investigate the impacts of changing emissions and climate on Arctic Hg atmosphere-ocean cycling over the past 30 years. We evaluate the model using long-term atmospheric Hg records and present-day oceanic Hg observations (as there are no data on temporal changes in Arctic seawater). We then use the model to gain insight into the environmental drivers of change in atmospheric and oceanic Hg and the implications for future climate change.

2. The GEOS-Chem Hg Model

[10] We use the GEOS-Chem Hg model v9-01-02 (http://geos-chem.org) to simulate atmospheric and surface ocean Hg over a 30 year period (1979–2008). Meteorological and other physical parameters driving the model are from the Modern Era Retrospective-analysis for Research and Applications (MERRA), a consistent assimilated data set produced by the NASA Global Modeling and Assimilation Office for that 30 year period [*Rienecker et al*., 2011]. The native horizontal resolution of the MERRA variables is $0.5° \times 0.667°$, which we downgrade to $4° \times 5°$ for input to GEOS-Chem. Temporal resolution is 3-hourly for 3-D variables (e.g., air temperature) and hourly for 2-D variables (e.g., sea ice fraction, surface temperature, and boundary layer depth). We compared trends and IAV of MERRA surface temperatures to the Goddard Institute for Space Studies analysis [*Hansen et al*., 2010] and found consistency over the Arctic during the entire 30 year simulation period. We also evaluated MERRA sea ice trends and IAV against passive microwave data from the National Snow and Ice Data Center (NSIDC) [*Comiso and Nishio*, 2008]. In summer, the MERRA sea ice product includes a correction to account for low bias in the passive microwave data caused by surface melt ponds [*Reynolds et al*., 2002]; as a result, MERRA summer ice concentrations are roughly 5% higher than the observations. In all other months, MERRA and NSIDC sea ice products are consistent (normalized mean bias $< 2\%$).

[11] The standard GEOS-Chem Hg model has been described in detail by *Holmes et al*. [2010], *Soerensen et al*. [2010], and *Amos et al*. [2012]. The model consists of a 3-D atmosphere dynamically coupled to a 2-D surface slab ocean

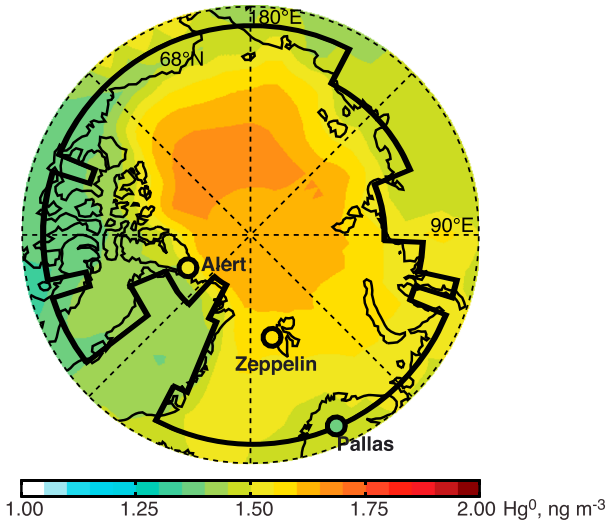

Figure 1. Mean 1995–2008 Hg^0 concentration in surface air simulated by GEOS-Chem. Observed long-term means from surface stations are also shown (Alert: 1995–2008, Pallas: 1996–2008, and Zeppelin: 2000–2008). The solid black line delineates the Arctic Ocean air mass as used here for model analyses (see text for definition). Here and in successive figures, observations are from *Cole et al.* [2013] at Alert (http://www.on.ec.gc.ca/natchem), *Berg et al.* [2013] at Zeppelin (http://ebas.nilu.no), and *Aas and Breivik* [2012] at Pallas (http://ebas.nilu.no).

and 2-D soil reservoir. Atmospheric processes include oxidation of Hg^0 by bromine atoms, photoreduction of Hg^{II} in liquid cloud droplets, gas-aerosol thermodynamic partitioning of Hg^{II}, and dry and wet deposition. The ocean mixed layer simulation includes redox chemistry driven by photochemical and biological processes, exchange with the atmosphere, aqueous-solid phase Hg^{II} partitioning, particulate settling, and mixing with subsurface waters where fixed concentrations are assumed. Ocean mixed layer depth in the central Arctic is defined based on 5 years of profile observations [*Toole et al.*, 2010] and varies from 15 m in summer to 20 m in winter. Elsewhere, a gridded interpolated climatology with monthly resolution is used [*de Boyer Montégut et al.*, 2004]. Horizontal transport in the ocean mixed layer is not considered.

[12] Application of the model to present-day simulation of the Arctic is detailed in *Fisher et al.* [2012]. Several updates were necessary to simulate changing conditions over the past three decades. These include use of the global historical anthropogenic emissions inventory of *Streets et al.* [2011], updates to bromine radical generation, implementation of UVB dependence for Hg^{II} photoreduction in seawater, new seasonal and interannual variation in Arctic Ocean net primary productivity distributions, and introduction of time-varying riverine inputs. All updates are described in detail in the supporting information.

3. Atmospheric Hg Trends and Variability

[13] Long-term atmospheric observations are available from three sites: 1995–2008 from Alert, Canada (83°N, 62°W, 205 m asl; [*Steffen et al.*, 2005]); 1996–2008 from Pallas, Finland (68°N, 26°E, 566 m asl; [*Berg et al.*, 2001]); and 2000–2008 from Zeppelin, Ny Ålesund, Svalbard (79°N, 12°E, 474 m asl; [*Berg et al.*, 2008]). Figure 1 shows the mean atmospheric Hg^0 concentration in Arctic surface air simulated by GEOS-Chem over the period of observational record. Concentrations are higher in the Arctic than at northern midlatitudes, consistent with observations and reflecting the source from the Arctic Ocean [*Andersson et al.*, 2008; *Hirdman et al.*, 2009; *Fisher et al.*, 2012]. Given the uniform treatment of processes in the surface ocean, GEOS-Chem does not attempt to resolve the horizontal variability of Hg across the Arctic. We will therefore focus much of our model analysis on mean budgets for the Arctic Ocean domain shown in Figure 1. This domain is defined as all 68°N–90°N GEOS-Chem grid squares with at least 20% ocean area. Pallas is just outside the domain boundary and is used here as a boundary condition to distinguish between Arctic and sub-Arctic behavior.

3.1. Seasonal Cycle

[14] Figure 2 shows the mean seasonal cycle of Hg^0 concentrations at each site. Both the observations and the model at Alert and Zeppelin display a spring minimum driven by AMDEs [*Cole and Steffen*, 2010; *Berg et al.*, 2013] and a summer maximum driven by evasion from the Arctic Ocean [*Hirdman et al.*, 2009; *Fisher et al.*, 2012]. The seasonality is damped at Zeppelin relative to Alert, reflecting the higher altitude (often outside the Arctic boundary layer). Pallas does not feature these Arctic signatures and shows instead a seasonality typical of northern midlatitudes, with a weak summer minimum driven by photochemical loss [*Selin et al.*, 2007].

[15] The GEOS-Chem Arctic mean simulation (blue) reproduces key features of the observed seasonal cycle. The model simulation at Alert (red) differs substantially from the modeled Arctic mean, with a sharper spring minimum and a weaker, delayed summer maximum. This reflects extensive and persistent local sea ice, leading to intense AMDE chemistry in spring and limited evasion in summer. The Arctic mean model value closely reproduces the summer peak at Alert, but the local value better reproduces the spring minimum. This could reflect a MERRA overestimate of summer sea ice at Alert, possibly due to the correction applied to account for surface melt ponds [*Reynolds et al.*, 2002]. A sensitivity test with local summer sea ice reduced by 15% showed an increase in simulated peak summer Hg^0 of ~0.1 ng m^{-3}. Additional model bias may arise from the complex topography at Alert, which in the model is located in a grid square with only 50% ocean fraction. Peak summer concentrations in the grid square north of Alert (100% ocean fraction) show a closer match to observations, with peak summer Hg^0 of ~2 ng m^{-3}.

[16] The model underestimates observations at Zeppelin for the second half of the year, both in the Zeppelin grid box and in the Arctic mean. The summer bias disappears if the model is sampled in surface air, suggesting an overly strong simulated vertical gradient. Simulated summer boundary layer heights at Zeppelin are usually lower than the 475 m elevation of the measurement site, despite observations that the station is usually located within the boundary layer in summer [*Sharma et al.*, 2012]. This discrepancy likely reflects grid-scale heterogeneity in surface type (land versus water) and associated differences in boundary layer dynamics,

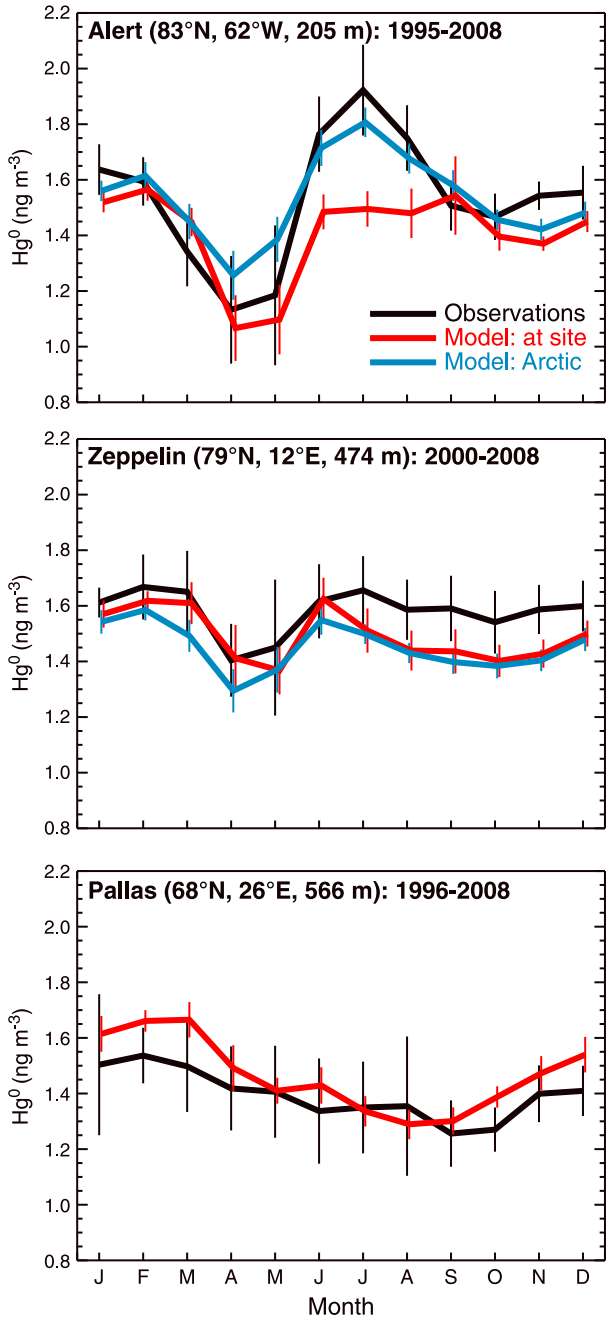

Figure 2. Seasonal cycle of atmospheric Hg^0 concentration at Alert, Zeppelin, and Pallas. Observed and modeled monthly mean concentrations are averaged over all available years of data through 2008 for each site. Vertical lines show the interannual variability defined as the standard deviation of the monthly mean concentrations. The black lines show the observed values, and the red lines show the GEOS-Chem simulation sampled at the grid box containing the location of the site (accounting for latitude, longitude, and elevation). The blue lines for Alert and Zeppelin indicate the area-weighted model mean for the Arctic Ocean air mass (Figure 1), sampled at the elevation of the site. Modeled values are offset slightly along the *x* axis to improve visibility.

as well as occasional missing inversions and overly cold surface temperatures in MERRA [*Jakobson et al.*, 2012; *Chung et al.*, 2013].

3.2. Long-Term Trends and Interannual Variability

[17] Observed long-term trends in Arctic atmospheric Hg^0 are weak. *Cole et al.* [2013] found that annual mean Hg^0 concentrations at Alert decreased by 0.01 ng m^{-3} a^{-1} over 2000–2009, while no significant trend was seen at Zeppelin [*Berg et al.*, 2013]. At both sites, trends differed greatly from month to month. In spring and summer, trends at both sites were generally positive (except in June) but were only significantly different from zero in May (+0.03 ng m^{-3} a^{-1}). GEOS-Chem simulates small increasing trends in all months (≤0.03 ng m^{-3} a^{-1}), which mainly reflects the growth in emissions in the *Streets et al.* [2011] inventory. Modeled trends (since 1990) would be negligible using the United Nations Environment Programme inventory (not used in the 30 year simulation as emissions are only available from 1990) [*United Nations Environment Programme*, 2013]. Trends would be negative if we accounted for decreasing evasion of Hg from the North Atlantic due to declining subsurface seawater concentrations [*Soerensen et al.*, 2012] and for decreasing release of Hg from commercial products [*Horowitz et al.*, 2013].

[18] The long-term trends are small relative to observed IAV, which is not influenced by the choice of emissions inventory. In all months, IAV is greater than 0.10 ng m^{-3} and can be as large as 0.25 ng m^{-3} (vertical lines in Figure 2). IAV at the high Arctic sites peaks in spring to summer (April–July), and we focus further analysis on these seasons when the Arctic atmosphere displays a unique signature. Fall and winter concentrations in the Arctic are more similar to those at northern midlatitudes [*Holmes et al.*, 2010], as illustrated in Figure 2 by comparison to Pallas. At Alert, peak IAV in April–May is driven primarily by the timing of the spring minimum, discussed below. Hg^0 at Zeppelin displays less IAV, as expected from the higher elevation and associated damping of surface processes. The large IAV at Zeppelin in May is driven by a low outlier from the first year of observations. In general, GEOS-Chem shows less IAV than the observations in part because of the coarse horizontal resolution, which results in average model values that dampen small-scale spatial variability. Simulated IAV shows the same seasonality as the observations, with peak IAV in spring due to AMDEs followed by reduced IAV in later months.

[19] The multiyear time series of observed atmospheric Hg^0 at Alert and Zeppelin are shown in Figure S1, with concentrations averaged over 2 month periods. Spring (April–May) and summer (June–July) are highlighted. The spring minimum and summer maximum occur in all years at Alert. At Zeppelin, behavior is more variable, and some years show no spring minimum or summer maximum. Figure 3 shows the time series of observed spring and summer Hg^0 at both sites, along with the simulated values averaged over the Arctic Ocean air mass. The figure indicates that behavior between the two sites is generally not coherent. Simulated Arctic mean Hg^0 falls between the two with lower IAV, caused in part by the Arctic-scale regional averaging. The simulated Arctic mean reproduces observed IAV with moderate success in spring (Alert $r = 0.41$, Zeppelin $r = 0.48$) and summer (Alert

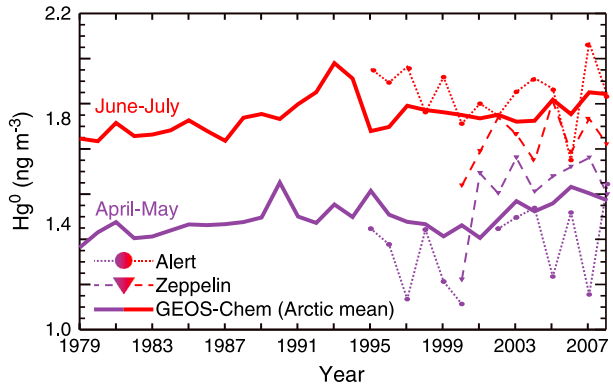

Figure 3. Time series of spring (April–May, purple) and summer (June–July, red) Hg^0 in Arctic surface air observed at Alert (dotted/circles), Zeppelin (dashed/triangles), and as simulated by GEOS-Chem (solid). GEOS-Chem values represent the area-weighted mean over the Arctic Ocean (Figure 1), sampled in surface air. Note that Alert (205 m above sea level) is located in the model's surface level, but Zeppelin (474 m above sea level) is in a higher level.

$r = 0.17$, Zeppelin $r = 0.47$). The factors controlling the model IAV will be discussed in section 4.

3.3. Timing of the Spring Minimum

[20] *Cole and Steffen* [2010] reported that the timing of the spring Hg minimum at Alert shifted from May in 1995–2001 to April in 2002–2007, which they attributed to a change in the timing of AMDEs caused by changes in local temperature. Figure 4 shows that this change is reproduced by the GEOS-Chem simulation sampled at Alert, although the magnitude of the change is weaker in the model. While the observed shift is driven by both an increase in May ($+0.33\ ng\ m^{-3}$) and a decrease in April ($-0.16\ ng\ m^{-3}$), the modeled shift is driven primarily by the May increase ($+0.11\ ng\ m^{-3}$), with little change in April ($-0.04\ ng\ m^{-3}$). As seen in Figure 4, the model is also generally able to reproduce the IAV in the difference between April and May Hg^0 concentration at Alert (model versus observation $r = 0.69$). Consistent with the findings of *Cole and Steffen* [2010], model correlation analysis shows that this IAV is driven by the April–May difference in surface air temperature ($r = 0.89$). On average, May at Alert was warmer in 2002–2007 than 1995–2001, while April was colder. The May warming has suppressed the temperature-dependent release of BrO while the April cooling has enhanced it, driving the observed shift in AMDE timing.

[21] At Zeppelin, there is no trend in the timing of the spring minimum in either the observations [*Cole et al.*, 2013] or the model. *Cole et al.* [2013] also show no trend over the past decade in the April–May difference at Kuujjuarapik (55°N, 78°W), a sub-Arctic site on Hudson Bay that also experiences AMDEs. More broadly, we find in GEOS-Chem no significant long-term trend in April–May differences for the mean Arctic Ocean air mass. This is true both for the 1995–2007 period analyzed by *Cole and Steffen* [2010] and for the full 30 year simulation. It suggests that the shift observed at Alert is not an Arctic-wide phenomenon but instead reflects local-scale forcing, including April atmospheric cooling at Alert that is opposite the temperature change observed for the Arctic mean [*Manabe et al.*, 2011].

4. Factors Driving Hg Interannual Variability in the Atmosphere

[22] We explored the potential drivers of Hg^0 IAV in Arctic surface air in spring and summer by correlation with a range of variables, including air temperature, sea ice fraction, planetary boundary layer depth, shortwave radiation, wind speed, ozone column, freshwater discharge, net primary productivity, and the Arctic Oscillation Index (details given in Table S1). Meteorological variables are from the MERRA assimilated data set. We also include freshwater discharge (see supporting information) and the Arctic Oscillation Index (from the NOAA Climate Prediction Center). The sensitivity of our results to the assumed Hg flux from circumpolar rivers is discussed in section S3 of the supporting information.

[23] The 30 year time series of April–May and June–July means for each driving variable in spring and summer, averaged over the Arctic Ocean air mass, are shown in Figure S2.

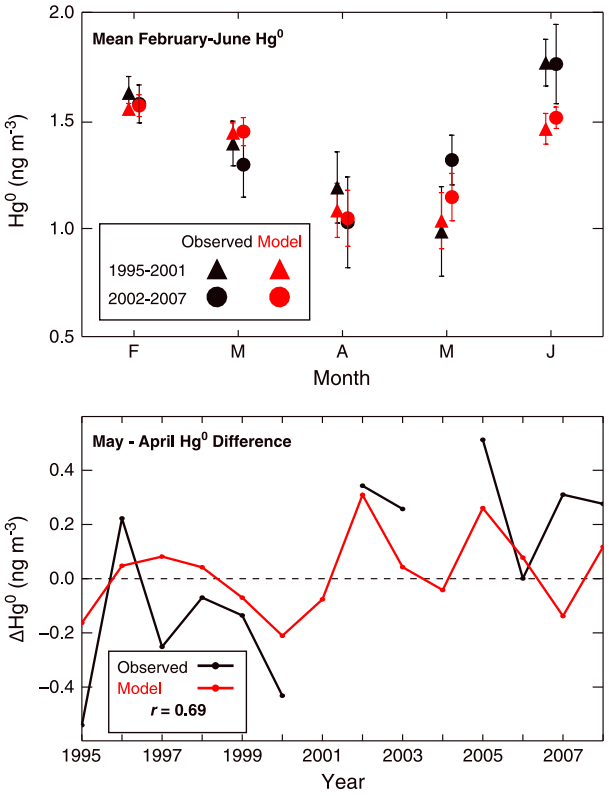

Figure 4. Seasonal shift of the spring minimum of Hg^0 concentration at Alert. Model values (red) are compared to observations (black). Figure 4 (top) shows monthly mean February–June concentrations for the two periods analyzed by *Cole and Steffen* [2010]: 1995–2001 (triangles) and 2002–2007 (circles). Vertical bars show the standard deviations of the monthly mean concentrations over these periods. Values are offset slightly along the *x* axis to improve visibility. Figure 4 (bottom) shows the time series of the difference (Δ) between May and April concentrations at Alert. The model-observation correlation coefficient (*r*) is given inset.

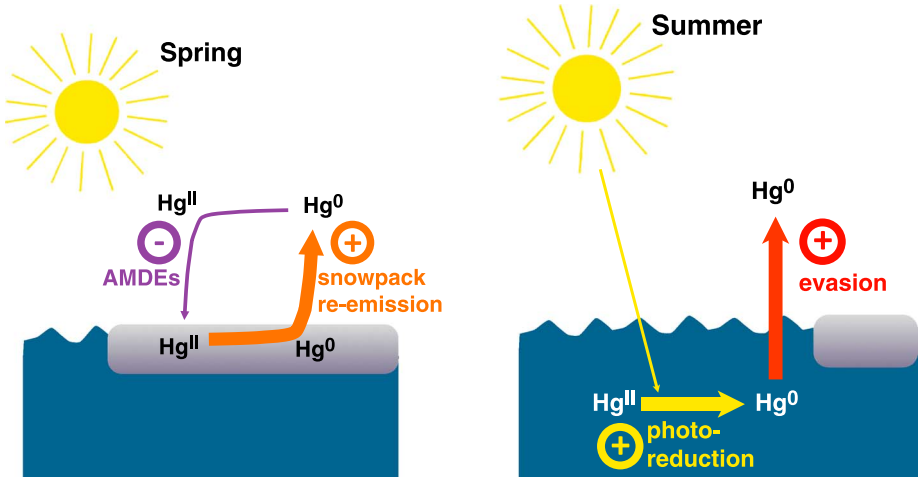

Figure 5. Impacts of the dominant Arctic climate mode driving atmospheric Hg^0 interannual variability in spring (left) and summer (right). The panels show mechanistically how positive phases of the mode impact relevant processes in each season, with (+) indicating a positive response and (−) indicating a negative response.

For most variables, IAV is much larger than the 30 year trend. Temperature shows minor IAV but significant increasing trends (computed using the nonparametric Sen's method [*Gilbert*, 1987]) of up to 1°C per decade in both seasons. Sea ice variables show moderate IAV and significant but small decreasing trends. The remaining meteorological variables display no long-term trends but substantial IAV. Observed long-term trends since 1980 in annual freshwater discharge of 10 km^3 a^{-1} are small (~0.5% a^{-1}) [*Shiklomanov and Lammers*, 2009]. The trend appears to be driven exclusively by changes in October–April flow, which is of little consequence for Hg cycling because total discharge is extremely low in these months [*Leitch et al.*, 2007; *Graydon et al.*, 2009; *Fisher et al.*, 2012]. We find no significant trends in monthly freshwater discharge from Russian rivers in the high flow months of May, June, or July. There is, however, large IAV in freshwater discharge.

[24] Correlation between the environmental variables of Table S1 and observed atmospheric Hg^0 concentrations at Alert and Zeppelin yielded few statistically significant relationships. At Alert, the only significant correlation was an inverse relationship with river discharge in spring, which is unlikely to reflect causality. This lack of identifiable drivers is consistent with the previous analysis by *Cole and Steffen* [2010], who found that monthly AMDE frequency was not correlated with wind speed, sea ice area, climate indices, or monthly mean temperature, although they did report a significant correlation with temperature when using hourly data. In summer, they found that low temperatures and low wind speeds were associated with elevated atmospheric Hg^0 but provided no information on the significance of these relationships.

[25] Using hourly Zeppelin observations (as opposed to the 2 month means used here), *Berg et al.* [2013] found a positive correlation between Hg^0 concentration and air temperature in April–May (but no strong correlations with wind speed, humidity, ozone column, or climate indices). The Hg^0-T relationship is obscured here by averaging the observations over 2 months. In summer, we find that observed Hg^0 at Zeppelin is weakly correlated ($r = 0.3$) with surface air temperature and anticorrelated ($r = -0.5$) with the depth of the planetary boundary layer (PBL). The latter reflects the importance of the ocean source of Hg, which remains trapped near the surface when the PBL is shallow.

[26] The lack of strong correlations between observed atmospheric Hg^0 and local meteorological variables found here and in other studies [*Cole and Steffen*, 2010; *Berg et al.*, 2013] suggests that Arctic Hg is influenced by nonlocal drivers. The GEOS-Chem simulation allows us to integrate these influences over the Arctic Ocean air mass. Our model analysis is necessarily limited to interpretation of these large-scale, nonlocal drivers. As discussed in section 3, the simulation underestimates observed variability at individual sites, which differs between Alert and Zeppelin and therefore reflects some additional forcing from local drivers that have not yet been identified. Nonetheless, as the model is able to capture much of the coherent variability between the two sites (simulated Arctic mean versus observed Alert-Zeppelin mean $r = 0.62$ in spring, $r = 0.55$ in summer), the model can provide useful insight on the Arctic-wide drivers of change.

[27] Using the full 30 year simulation, we find in both seasons that simulated mean Hg^0 concentration is positively correlated with temperature (consistent with the observations [*Cole and Steffen*, 2010; *Berg et al.*, 2013]) and solar radiation and negatively correlated with sea ice fraction, PBL depth, and ozone column. In spring, we find an additional positive correlation with wind speed. These relationships hint at a number of potential driving processes; however, the meteorological variables are themselves strongly correlated with one another (e.g., high air temperature is associated with low sea ice fraction, high radiation, and shallow PBL depth), complicating process-based identification from correlation analysis alone.

[28] We therefore performed a principal component analysis (PCA) (see supporting information) of the variables shown in Table S1. The resulting orthogonal principal components (PCs) represent distinct climatic modes. Figure S3 shows the composition of the dominant PC for each season.

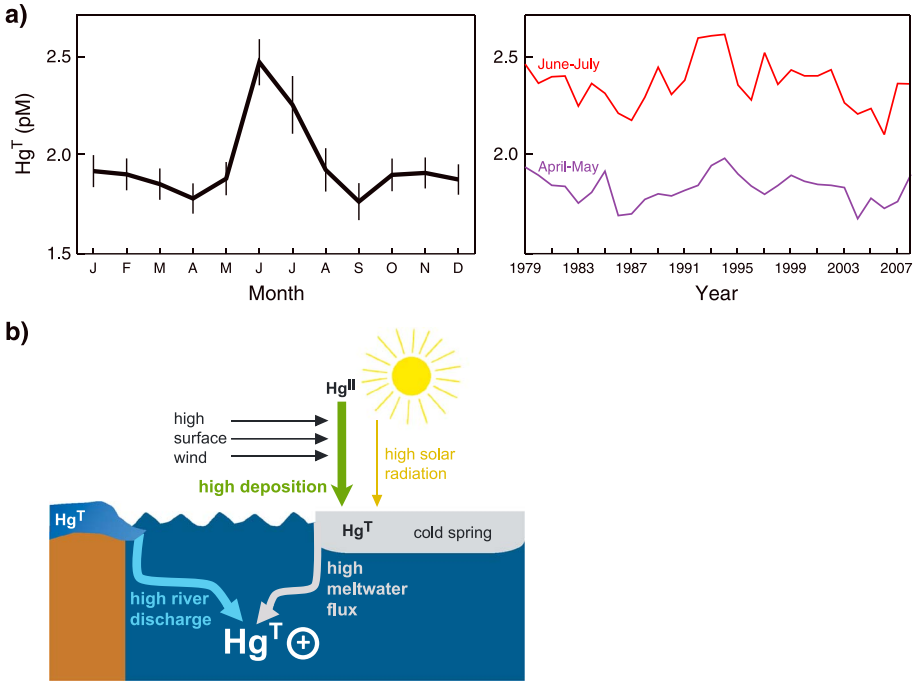

Figure 6. (a) Total mercury (Hg^T) concentration (pM) in surface waters of the Arctic Ocean (68°N–90°N) as simulated by GEOS-Chem. Figure 6a (left) shows the mean seasonal cycle, averaged over 1979–2008, with vertical lines indicating the interannual variability defined as the standard deviation of the monthly mean concentrations. Figure 6a (right) shows the 30 year (1979–2008) time series for spring (April–May, purple) and summer (June–July, red). (b) Principal environmental variables driving interannual variability of simulated total mercury (Hg^T) concentrations in the Arctic Ocean mixed layer in summer. Conditions shown here lead to elevated Hg^T.

Major meteorological contributions to the dominant PC are consistent with the correlation analysis. In both seasons, the dominant mode is associated with high temperature, low sea ice fraction, high solar radiation, and low PBL height over ice. The latter reflects a strong anticorrelation between temperature and PBL height induced by warm air over cold sea ice forcing atmospheric stratification. The positive mode also shows an association with high net primary productivity (NPP), but this mainly reflects strong correlation between NPP, air temperature, and sea ice fraction driven by the NPP IAV parameterization. Together, contributions to this PC point to a climatological origin for the dominant mode, with positive values of this mode associated with "warm" years driving increased atmospheric Hg^0, while low values associated with "cold" years lead to decreased atmospheric Hg^0.

[29] The schematics in Figure 5 show for each season how the relevant processes combine to increase atmospheric Hg^0 in positive phases of the dominant mode. In spring, high temperatures and low sea ice fractions drive fewer AMDEs and therefore less Hg removal from the atmosphere. Simultaneously, high solar radiation drives increased snowpack photoreduction and therefore more reemission of Hg to the atmosphere. In summer, high solar radiation leads to increased Hg^0 formation via photoreduction in the surface ocean, accompanied by increased open water area (low sea ice fraction) driving enhanced Hg^0 evasion. Principal component regression of the PCs (see supporting information) to our 30 year simulation indicates that the first PC accounts for 83% of the IAV in simulated Hg^0 concentration in spring ($r = 0.91$) and 40% in summer ($r = 0.63$). The second PC (dominated by high wind speed) explains an additional 13% of simulated summer IAV. The dominant PCs are weakly correlated with observed Hg^0 in both spring ($r = 0.22$ at Alert, $r = 0.30$ at Zeppelin) and summer ($r = 0.36$ at Alert, $r = 0.33$ at Zeppelin). The correlation is improved to $r \cong 0.3$–0.4 in spring if the PC is computed without including ozone column. The total ozone column is dominated by stratospheric ozone and is used here as an indication of the impact on aqueous Hg photochemistry of UVB modulation driven by stratospheric ozone loss and recovery. We therefore do not expect ozone column to influence Arctic Hg in spring, when atmospheric concentrations are not driven by the ocean source.

5. Factors Driving Hg Interannual Variability in the Surface Ocean

[30] Figure 6a shows the mean simulated seasonal cycle and 30 year time series of April–May and June–July total mercury (Hg^T) concentration in surface waters of the Arctic Ocean. Ocean Hg is low in spring following mixing with subsurface waters and peaks in June due to large riverine inputs [*Fisher et al.*, 2012]. Mean peak simulated concentrations of $Hg^T = 2.5$ pM in the surface ocean are consistent with the limited available Arctic surface water observations from *Kirk et al.* [2008] ($Hg^T = 2.9 \pm 2.9$ pM), *Lehnherr et al.* [2011] ($Hg^T = 1.8 \pm 0.7$ pM), and *Wang et al.* [2012] (Hg^T range 1.0–2.9 pM). Mean peak simulated $Hg^0 = 0.21$ pM occurs in July and is somewhat higher than observed by *Kirk et al.* [2008] in August–September ($Hg^0 = 0.13 \pm 0.05$ pM), reflecting the seasonal decrease shown in Figure 6a. Peak modeled

Hg^0 is more closely aligned with July–September observations of 0.22 ± 0.11 pM from *Andersson et al.* [2008], although this value is for total dissolved gaseous mercury and includes an unquantified contribution from dimethyl Hg (not simulated in GEOS-Chem). Despite the assumed increases in Hg emissions to the atmosphere (supporting information), there is no statistically significant trend in modeled ocean Hg^T concentrations over the 1979–2008 period, although IAV is large.

[31] Oceanic Hg^T IAV peaks in summer (June–July) in the simulation (vertical lines in Figure 6a). Variability is limited during the rest of the year and tends to lag summer variability, suggesting that summertime processes are largely responsible for IAV in the surface ocean throughout the year. We find from the model that mean June–July Hg^T is most strongly correlated on an interannual basis with Hg inputs from melting snow on sea ice in June ($r = 0.73$), followed by Hg deposited directly to the ocean in spring ($r = 0.49$) and May Hg discharge from rivers ($r = 0.38$). Variability in the meltwater flux is largely controlled by variability in solar radiation ($r = 0.62$), which in summer is the dominant source of energy to sea ice [*Hudson et al.*, 2013]. Clear skies (driving increased shortwave radiation) can greatly enhance both surface and basal ice melt [*Kay et al.*, 2008], triggering a large input of Hg-enriched meltwater to the ocean. The meltwater flux is also large in years with a cold spring driving frequent AMDEs ($r = -0.37$). We find an additional positive correlation with wind speed ($r = 0.58$), which reflects increased deposition to sea ice via enhanced turbulent mixing of Hg-enriched air masses under high winds, further increasing the meltwater Hg reservoir. This effect is opposite to what is seen at midlatitudes, where higher wind speed decreases ocean Hg through enhanced evasion [*Soerensen et al.*, 2010]. Higher wind speeds also increase evasion in the Arctic, but this loss of oceanic Hg^0 is more than offset by the increase in Hg^{II} from deposition to sea ice.

[32] Figure 6a shows a peak in simulated ocean Hg^T in 1992–1994 driven by the combined influence of solar radiation and wind speed, which during those years were each 1–3 standard deviations above their summer means. The resultant elevated ocean Hg was sufficient to also drive a peak in atmospheric Hg^0 through enhanced evasion, as seen in Figure 3. Stepwise multiple linear regression (see supporting information) of simulated ocean Hg^T over the entire 30 year simulation shows that wind speed, solar radiation, May surface air temperature, and May freshwater discharge (in that order of importance) can together explain 55% of Hg^T variability. None of the other environmental variables in Table S1 are significant predictors for simulated Hg^T. In particular, sea ice fraction does not correlate with Hg^T because of competing effects from meltwater input and evasive loss (both increased when ice fraction is low). The mechanisms relating Hg^T to the four explanatory variables are illustrated in Figure 6b. These variables are only weakly correlated with one another, and we find no additional information from a principal component analysis.

6. Conclusions and Implications for the Effects of Climate Change

[33] We have used a 1979–2008 simulation of the Arctic Hg cycle in the GEOS-Chem global biogeochemical Hg model, together with long-term atmospheric observations of elemental mercury (Hg^0) concentrations at Alert (1995–2008) and Zeppelin (2000–2008), to examine the factors driving the 30 year interannual variability (IAV) of Hg in the Arctic atmosphere and ocean. Long-term atmospheric trends in the Alert and Zeppelin records are marginal or insignificant, but there is large IAV that offers insight into the potential effects of climate change. No long-term observational records exist for Hg in the Arctic Ocean, but some insight into the driving processes can be gained from the GEOS-Chem simulation.

[34] Atmospheric observations at Alert and Zeppelin show an April–May spring minimum due to atmospheric mercury depletion events (AMDEs) involving halogen chemistry over broken sea ice and a June–July summer maximum due to ocean evasion. The model reproduces these features. IAV in spring and summer is usually not coherent at Alert and Zeppelin, and the model shows moderate skill in reproducing it ($r \sim 0.4$). Observations at Alert show a shift from a May minimum in 1995–2001 to an April minimum in 2002–2007, a feature previously attributed by *Cole and Steffen* [2010] to local cooling in April and warming in May. The model reproduces this shift as well as the IAV of the April–May difference in Hg^0 concentrations at Alert and also attributes the shift to local cooling in April along with warming in May. These local conditions are not characteristic of the Arctic as a whole, which has instead experienced warming in all months [*Manabe et al.*, 2011], and we find no shift in AMDE timing at Zeppelin or for the mean Arctic Ocean air mass.

[35] We examined the factors driving the IAV of Hg^0 in Arctic surface air through correlation with 11 climatological variables. Consistent with previous analyses [*Cole and Steffen*, 2010; *Berg et al.*, 2013], observations at Alert and Zeppelin show only weak correlations with local meteorological variables, hinting at nonlocal influences. Examination of spring and summer IAV in modeled Arctic mean Hg^0 indicates positive correlations with temperature and solar radiation and negative correlations with sea ice fraction, planetary boundary layer (PBL) depth, and ozone column. A principal component analysis (PCA) for the model fields indicates that Hg^0 IAV is largely driven by a single climate mode with the positive phase consisting of high temperatures, low sea ice fraction, high solar radiation (clear skies), and shallow PBL. In spring, these factors combine to decrease the frequency and intensity of AMDEs while enhancing the photoreduction and reemission of Hg deposited to snowpacks, driving increased atmospheric Hg^0. In summer, this mode drives increased photoreduction of Hg^{II} in the ocean followed by enhanced evasion of Hg^0 to the atmosphere. Model underestimates of observed IAV at Alert and Zeppelin suggest some additional influence from local drivers not yet identified.

[36] Examination of the factors driving the IAV of summertime total mercury (Hg^T) in the Arctic Ocean mixed layer in the model indicates a dominant influence from the meltwater flux of Hg previously deposited to snow on sea ice, with secondary influence from spring deposition to the ocean and river inputs. The strength of the meltwater flux is in turn linked to climate parameters, with higher fluxes seen in years with high solar radiation (clear skies) driving ice melt, high wind speed driving increased deposition, and cold spring air temperature driving enhanced AMDE deposition to sea ice. A sensitivity simulation with the riverine Hg flux decreased by a factor of 10 showed limited impact on simulated IAV and its drivers due to the seasonal offset between peak IAV and peak flow (supporting information).

[37] These results have important implications for the future of Arctic Hg cycling. We have shown that decreased fluxes of Hg from the atmosphere to the cryosphere and from the cryosphere to the ocean are associated with changes induced by climate warming: high air temperatures, low sea ice area, strong warming in spring [*Bekryaev et al*., 2010], and cloudiness [*Eastman and Warren*, 2010]. These changes are projected to intensify under future forcing scenarios [*Intergovernmental Panel on Climate Change*, 2007; *Vavrus et al*., 2009], suggesting future climate change may decrease Hg levels in the Arctic surface ocean. However, key uncertainties remain in our understanding of Hg inputs to the Arctic Ocean. Better empirical constraints are needed for the magnitude of riverine inputs and the direction of change associated with the transforming Arctic landscape, as well as for evolving inputs from changing seawater Hg concentrations in the Atlantic and Pacific basins [*Sunderland et al*., 2009; *Soerensen et al*., 2012]. Linking climate-driven changes in inorganic Hg cycling to accumulation in Arctic Ocean food webs requires integration of the findings presented here with better understanding of temporal changes in methylmercury production, uptake, and trophic transfer.

[38] **Acknowledgments.** This work was supported by the NSF Office of Polar Programs. JAF acknowledges support from a University of Wollongong Vice Chancellor's Postdoctoral Fellowship. ALS acknowledges support from the Carlsberg Foundation. We thank A. Steffen, A. Cole, and the Canadian National Atmospheric Chemistry Database for the collection and provision of the Alert data, with financial support provided by the Northern Contaminants Program, Environment Canada, and the Arctic Monitoring and Assessment Programme. We also thank the European Monitoring and Evaluation Programme, the Finnish Meteorological Institute, and the Norwegian Institute for Air Research for the collection and provision of the Zeppelin and Pallas data. MERRA data used in this study have been provided by the Global Modeling and Assimilation Office at NASA Goddard Space Flight Center through the NASA GES DISC online archive. We thank A. Qureshi for helpful discussions.

References

Aas, W., and K. Breivik (2012), Heavy metals and POP measurements, 2010, EMEP/CCC-Report 3/2012, Norwegian Institute for Air Research, Kjeller, Norway.

Amos, H. A., et al. (2012), Gas-particle partitioning of atmospheric Hg(II) and its effect on global mercury deposition, *Atmos. Chem. Phys.*, *12*, 591–603, doi:10.5194/acp-12-591-2012.

Andersson, M., J. Sommar, K. Gårdfeldt, and O. Lindqvist (2008), Enhanced concentrations of dissolved gaseous mercury in the surface waters of the Arctic Ocean, *Mar. Chem.*, *110*(3–4), 190–194, doi:10.1016/j.marchem.2008.04.002.

Ariya, P. A., A. P. Dastoor, M. Amyot, W. H. Schroeder, L. Barrie, K. Anlauf, F. Raofie, A. Ryzhkov, D. Davignon, and J. Lalonde (2004), The Arctic: A sink for mercury, *Tellus B*, *56*(5), 397–403.

Arrigo, K. R., and G. L. van Dijken (2011), Secular trends in Arctic Ocean net primary production, *J. Geophys. Res.*, *116*, C09011, doi:10.1029/2011JC007151.

Atkinson, D. E. (2005), Observed storminess patterns and trends in the circum-Arctic coastal regime, *Geo-Mar Lett*, *25*(2–3), 98–109, doi:10.1007/s00367-004-0191-0.

Bais, A. F., et al. (2011), Projections of UV radiation changes in the 21st century: Impact of ozone recovery and cloud effects, *Atmos. Chem. Phys.*, *11*(15), 7533–7545, doi:10.5194/acp-11-7533-2011.

Bekryaev, R. V., I. V. Polyakov, and V. A. Alexeev (2010), Role of polar amplification in long-term surface air temperature variations and modern arctic warming, *J. Clim.*, *23*(14), 3888–3906, doi:10.1175/2010JCLI3297.1.

Berg, T., J. Bartnicki, J. Munthe, H. Lattila, J. Hrehoruk, and A. Mazur (2001), Atmospheric mercury species in the European Arctic: Measurements and modelling, *Atmos. Environ.*, *35*(14), 2569–2582.

Berg, T., K. Aspmo, and E. Steinnes (2008), Transport of Hg from Atmospheric mercury depletion events to the mainland of Norway and its possible influence on Hg deposition, *Geophys. Res. Lett.*, *35*, L09802, doi:10.1029/2008GL033586.

Berg, T., K. A. Pfaffhuber, A. S. Cole, O. Engelsen, and A. Steffen (2013), Ten-years trends in atmospheric mercury concentrations, meteorological effects and climate variables at Zeppelin, Ny-Ålesund, *Atmos. Chem. Phys.*, *13*, 6575–6586.

Bintanja, R., R. G. Graversen, and W. Hazeleger (2011), Arctic winter warming amplified by the thermal inversion and consequent low infrared cooling to space, *Nat. Geosci.*, *4*(11), 758–761, doi:10.1038/NGEO1285.

de Boyer Montégut, C., G. Madec, A. S. Fischer, A. Lazar, and D. Iudicone (2004), Mixed layer depth over the global ocean: An examination of profile data and a profile-based climatology, *J. Geophys. Res.*, *109*, C12003, doi:10.1029/2004JC002378.

Cavalieri, D. J., and C. L. Parkinson (2012), Arctic sea ice variability and trends, 1979–2010, *The Cryosphere*, *6*(4), 881–889, doi:10.5194/tc-6-881-2012.

Chung, C. E., H. Cha, T. Vihma, P. Räisänen, and D. Decremer (2013), On the possibilities to use atmospheric reanalyses to evaluate the warming structure in the Arctic, *Atmos. Chem. Phys.*, *13*, 11,209–11,219, doi:10.5194/acp-13-11209-2013.

Cole, A. S., and A. Steffen (2010), Trends in long-term gaseous mercury observations in the Arctic and effects of temperature and other atmospheric conditions, *Atmos. Chem. Phys.*, *10*, 4661–4672, doi:10.5194/acp-10-4661-2010.

Cole, A. S., A. Steffen, K. A. Pfaffhuber, T. Berg, M. Pilote, L. Poissant, R. Tordon, and H. Hung (2013), Ten-year trends of atmospheric mercury in the high Arctic compared to Canadian sub-Arctic and mid-latitude sites, *Atmos. Chem. Phys.*, *13*, 1535–1545, doi:10.5194/acp-13-1535-2013.

Comiso, J. C., and F. Nishio (2008), Trends in the sea ice cover using enhanced and compatible AMSR-E, SSM/I, and SMMR data, *J. Geophys. Res.*, *113*, doi:10.1029/2007JC004257.

Coquery, M., D. Cossa, and J. Martin (1995), The distribution of dissolved and particulate mercury in three Siberian estuaries and adjacent Arctic coastal waters, *Water Air Soil Pollut.*, *80*(1), 653–664.

Corbitt, E. S., D. J. Jacob, C. D. Holmes, D. G. Streets, and E. M. Sunderland (2011), Global source-receptor relationships for mercury deposition under present-day and 2050 emissions scenarios, *Environ. Sci. Technol.*, *45*(24), 10,477–10,484, doi:10.1021/es202496y.

Durnford, D., and A. Dastoor (2011), The behavior of mercury in the cryosphere: A review of what we know from observations, *J. Geophys. Res.*, *116*, D06305, doi:10.1029/2010JD014809.

Durnford, D., A. Dastoor, D. Figueras-Nieto, and A. Ryjkov (2010), Long range transport of mercury to the Arctic and across Canada, *Atmos. Chem. Phys.*, *10*, 6063–6086, doi:10.5194/acp-10-6063-2010.

Eastman, R., and S. G. Warren (2010), Interannual variations of arctic cloud types in relation to sea ice, *J. Clim.*, *23*, 4216–4232, doi:10.1175/2010JCLI3492.1.

Emmerton, C. A., J. A. Graydon, J. A. L. Gareis, V. L. St Louis, L. F. W. Lesack, J. K. A. Banack, F. Hicks, and J. Nafziger (2013), Mercury export to the Arctic Ocean from the Mackenzie River, Canada, *Environ. Sci. Technol.*, *47*, 7644–7654, doi:10.1021/es400715r.

Fisher, J. A., D. J. Jacob, A. L. Soerensen, H. A. Amos, A. Steffen, and E. M. Sunderland (2012), Riverine source of Arctic Ocean mercury inferred from atmospheric observations, *Nat. Geosci.*, *5*, 499–504, doi:10.1038/NGEO1478.

Gilbert, R. O. (1987), *Statistical Methods for Environmental Pollution Monitoring*, John Wiley & Sons, Inc., New York.

Goodsite, M. E., J. M. C. Plane, and H. Skov (2004), A theoretical study of the oxidation of Hg0 to HgBr2 in the troposphere, *Environ. Sci. Technol.*, *38*, 1772–1776, doi:10.1021/es034680s.

Graydon, J. A., C. A. Emmerton, L. F. W. Lesack, and E. N. Kelly (2009), Mercury in the Mackenzie River delta and estuary: Concentrations and fluxes during open-water conditions, *Sci. Total Environ.*, *407*(8), 2980–2988, doi:10.1016/j.scitotenv.2008.12.060.

Hansen, J., R. Ruedy, M. Sato, and K. Lo (2010), Global surface temperature change, *Rev. Geophys.*, *48*, RG4004, doi:10.1029/2010RG000345.

Hirdman, D., K. Aspmo, J. F. Burkhart, S. Eckhardt, H. Sodemann, and A. Stohl (2009), Transport of mercury in the Arctic atmosphere: Evidence for a spring- time net sink and summer-time source, *Geophys. Res. Lett.*, *36*, L12814, doi:10.1029/2009GL038345.

Holmes, C. D., D. J. Jacob, E. S. Corbitt, J. Mao, X. Yang, R. Talbot, and F. Slemr (2010), Global atmospheric model for mercury including oxidation by bromine atoms, *Atmos. Chem. Phys.*, *10*, 12,037–12,057, doi:10.5194/acp-10-12037-2010.

Horowitz, H. M., D. J. Jacob, D. G. Streets, H. A. Amos, and E. M. Sunderland (2013), Global environmental release of mercury from commercial products, paper presented at International Conference on Mercury as a Global Pollutant, Edinburgh, Scotland.

Hudson, S. R., M. A. Granskog, A. Sundfjord, A. Randelhoff, A. H. H. Renner, and D. V. Divine (2013), Energy budget of first-year Arctic sea ice in advanced stages of melt, *Geophys. Res. Lett.*, *40*, 1–5, doi:10.1002/grl.50517.

Intergovernmental Panel on Climate Change (IPCC) (2007), *Climate Change 2007: The Physical Science Basis. Contribution of Working*

Group I to the Fourth Assessment Report of the Intergovernmental Panel on Climate Change, edited by S. Solomon et al., Cambridge Univ. Press, Cambridge, U. K., and New York.

Jakobson, E., T. Vihma, T. Palo, L. Jakobson, H. Keernik, and J. Jaagus (2012), Validation of atmospheric reanalyses over the central Arctic Ocean, *Geophys. Res. Lett.*, *39*, L10802, doi:10.1029/2012GL051591.

Kay, J. E., T. L'Ecuyer, A. Gettelman, G. Stephens, and C. O'Dell (2008), The contribution of cloud and radiation anomalies to the 2007 Arctic sea ice extent minimum, *Geophys. Res. Lett.*, *35*, L08503, doi:10.1029/2008GL033451.

Kirk, J. L., V. L. St. Louis, H. Hintelmann, I. Lehnherr, B. Else, and L. Poissant (2008), Methylated mercury species in marine waters of the Canadian high and sub Arctic, *Environ. Sci. Technol.*, *42*(22), 8367–8373, doi:10.1021/es801635m.

Klaminder, J., K. Yoo, J. Rydberg, and R. Giesler (2008), An explorative study of mercury export from a thawing palsa mire, *J. Geophys. Res.*, *113*, G04034, doi:10.1029/2008JG000776.

Kwok, R., and D. A. Rothrock (2009), Decline in Arctic sea ice thickness from submarine and ICESat records: 1958–2008, *Geophys. Res. Lett.*, *36*, L15501, doi:10.1029/2009GL039035.

Lantuit, H., et al. (2012), The Arctic coastal dynamics database: A new classification scheme and statistics on Arctic permafrost coastlines, *Estuar Coast*, *35*(2), 383–400, doi:10.1007/s12237-010-9362-6.

Lehnherr, I., V. L. St, H. H. Louis, and J. L. Kirk (2011), Methylation of inorganic mercury in polar marine waters, *Nat. Geosci.*, *4*, 298–302, doi:10.1038/NGEO1134.

Leitch, D. R. (2006), Mercury distribution in water and permafrost of the Lower Mackenzie Basin, their contribution to the mercury contamination in the Beaufort Sea marine ecosystem, and potential effects of climate variation, MSc thesis, University of Manitoba, Winnipeg, Manitoba.

Leitch, D. R., J. Carrie, D. Lean, R. W. Macdonald, G. A. Stern, and F. Wang (2007), The delivery of mercury to the Beaufort Sea of the Arctic Ocean by the Mackenzie River, *Sci. Total Environ.*, *373*(1), 178–195, doi:10.1016/j.scitotenv.2006.10.041.

Macdonald, R. W., T. Harner, and J. Fyfe (2005), Recent climate change in the Arctic and its impact on contaminant pathways and interpretation of temporal trend data, *Sci. Total Environ.*, *342*(1–3), 5–86, doi:10.1016/j.scitotenv.2004.12.059.

Manabe, S., J. Ploshay, and N.-C. Lau (2011), Seasonal variation of surface temperature change during the last several decades, *J. Clim.*, *24*, 3817–3821, doi:110.1175/JCLI-D-11-00129.1.

Munthe, J., et al. (2011), Where does mercury in the arctic environment come from, and how does it get there?, in *AMAP Assessment 2011: Mercury in the Arctic*, pp. 9–60, Arctic Monitoring and Assessment Programme, Oslo.

O'Donnell, J. A., G. R. Aiken, M. A. Walvoord, and K. D. Butler (2012), Dissolved organic matter composition of winter flow in the Yukon River basin: Implications of permafrost thaw and increased groundwater discharge, *Global Biogeochem. Cycle.*, *26*, GB0E06, doi:10.1029/2012GB004341.

O'Driscoll, N. J., S. D. Siciliano, D. R. S. Lean, and M. Amyot (2006), Gross photoreduction kinetics of mercury in temperate freshwater lakes and rivers: Application to a general model of DGM dynamics, *Environ. Sci. Technol.*, *40*(3), 837–843, doi:10.1021/es051062y.

Outridge, P., R. Macdonald, F. Wang, G. Stern, and A. Dastoor (2008), A mass balance inventory of mercury in the Arctic Ocean, *Environ. Chem.*, *5*(2), 89–111, doi:10.1071/EN08002.

Parkinson, C. L., and D. J. Cavalieri (2008), Arctic sea ice variability and trends, 1979–2006, *J. Geophys. Res.*, *113*, C07004, doi:10.1029/2007JC004564.

Piot, M., and R. von Glasow (2008), The potential importance of frost flowers, recycling on snow, and open leads for ozone depletion events, *Atmos. Chem. Phys.*, *8*(9), 2437–2467, doi:10.5194/acp-8-2437-2008.

Pöhler, D., L. Vogel, U. Frieß, and U. Platt (2010), Observation of halogen species in the Amundsen Gulf, Arctic, by active long-path differential optical absorption spectroscopy, *Proc. Natl. Acad. Sci. U.S.A.*, *107*(15), 6582–6587, doi:10.1073/pnas.0912231107.

Pratt, K. A., et al. (2013), Photochemical production of molecular bromine in Arctic surface snowpacks, *Nat. Geosci.*, *6*, 351–356, doi:10.1038/NGEO1779.

Reynolds, R. W., N. A. Rayner, T. M. Smith, D. C. Stokes, and W. Wang (2002), An improved in situ and satellite SST analysis for climate, *J. Clim.*, *15*, 1609–1625.

Rienecker, M. M., et al. (2011), MERRA: NASA's modern-era retrospective analysis for research and applications, *J. Clim.*, *24*(14), 3624–3648, doi:10.1175/JCLI-D-11-00015.1.

Rigét, F., et al. (2011), Temporal trends of Hg in Arctic biota, an update, *Sci. Total Environ.*, *409*(18), 3520–3526, doi:10.1016/j.scitotenv.2011.05.002.

Rydberg, J., J. Klaminder, P. Rosén, and R. Bindler (2010), Climate driven release of carbon and mercury from permafrost mires increases mercury loading to sub-arctic lakes, *Sci. Total Environ.*, *408*, 4778–4783, doi:10.1016/j.scitotenv.2010.06.056.

Screen, J. A., and I. Simmonds (2010), The central role of diminishing sea ice in recent Arctic temperature amplification, *Nature*, *464*(7293), 1334–1337, doi:10.1038/nature09051.

Selin, N. E., D. J. Jacob, R. J. Park, R. M. Yantosca, S. Strode, L. Jaeglé, and D. Jaffe (2007), Chemical cycling and deposition of atmospheric mercury: Global constraints from observations, *J. Geophys. Res.*, *112*, D02308, doi:10.1029/2006JD007450.

Sharma, S., et al. (2012), Influence of transport and ocean ice extent on biogenic aerosol sulfur in the Arctic atmosphere, *J. Geophys. Res.*, *117*, D12209, doi:10.1029/2011JD017074.

Shiklomanov, A. I., and R. B. Lammers (2009), Record Russian river discharge in 2007 and the limits of analysis, *Environ. Res. Lett.*, *4*, 045015, doi:10.1088/1748-9326/4/4/045015.

Simpson, W. R., D. Carlson, G. Hönniger, T. A. Douglas, M. Sturm, D. K. Perovich, and U. Platt (2007a), First-year sea-ice contact predicts bromine monoxide (BrO) levels at Barrow, Alaska better than potential frost flower contact, *Atmos. Chem. Phys.*, *7*, 621–627, doi:10.5194/acp-7-621-2007.

Simpson, W. R., R. von Glasow, K. Riedel, P. Anderson, P. Ariya, J. Bottenheim, J. Burrows, L. Carpenter, U. Frieß, and M. E. Goodsite (2007b), Halogens and their role in polar boundary-layer ozone depletion, *Atmos. Chem. Phys.*, *7*(16), 4375–4418, doi:10.5194/acp-7-4375-2007.

Slemr, F., G. Schuster, and W. Seiler (1985), Distribution, speciation, and budget of atmospheric mercury, *J. Atmos. Chem.*, *3*(4), 407–434.

Soerensen, A. L., E. M. Sunderland, C. D. Holmes, D. J. Jacob, R. M. Yantosca, H. Skov, J. H. Christensen, S. A. Strode, and R. P. Mason (2010), An improved global model for air-sea exchange of mercury: High concentrations over the North Atlantic, *Environ. Sci. Technol.*, *44*, 8574–8580, doi:10.1021/es102032g.

Soerensen, A. L., D. J. Jacob, D. G. Streets, M. L. I. Witt, R. Ebinghaus, R. P. Mason, M. Andersson, and E. M. Sunderland (2012), Multi-decadal decline of mercury in the North Atlantic atmosphere explained by changing subsurface seawater concentrations, *Geophys. Res. Lett.*, *39*, L21810, doi:10.1029/2012GL053736.

Sommar, J., M. E. Andersson, and H.-W. Jacobi (2010), Circumpolar measurements of speciated mercury, ozone and carbon monoxide in the boundary layer of the Arctic Ocean, *Atmos. Chem. Phys.*, *10*, 5031–5045, doi:10.5194/acp-10-5031-2010.

Steffen, A., W. Schroeder, R. Macdonald, L. Poissant, and A. Konoplev (2005), Mercury in the Arctic atmosphere: An analysis of eight years of measurements of GEM at Alert (Canada) and a comparison with observations at Amderma (Russia) and Kuujjuarapik (Canada), *Sci. Total Environ.*, *342*(1–3), 185–198, doi:10.1016/j.scitotenv.2004.12.048.

Steffen, A., et al. (2008), A synthesis of atmospheric mercury depletion event chemistry in the atmosphere and snow, *Atmos. Chem. Phys.*, *8*, 1445–1482, doi:10.5194/acp-8-1445-2008.

Stern, G. A., et al. (2012), How does climate change influence arctic mercury?, *Sci. Total Environ.*, *414*, 22–42, doi:10.1016/j.scitotenv.2011.10.039.

Stow, J., E. Krümmel, T. Leech, and S. Donaldson (2011), What is the impact of mercury contamination on human health in the Arctic?, in *AMAP Assessment 2011: Mercury in the Arctic*, edited, pp. 159–170, Arctic Monitoring and Assessment Programme, Oslo.

Streets, D. G., M. K. Devane, Z. F. Lu, T. C. Bond, E. M. Sunderland, and D. J. Jacob (2011), All-time releases of mercury to the atmosphere from human activities, *Environ. Sci. Technol.*, *45*(24), 10,485–10,491, doi:10.1021/es202765m.

Sunderland, E. M., D. P. Krabbenhoft, J. W. Moreau, S. Strode, and W. M. Landing (2009), Mercury sources, distribution, and bioavailability in the North Pacific Ocean: Insights from data and models, *Global Biogeochem. Cycle.*, *23*, GB2010, doi:10.1029/2008GB003425.

Toole, J. M., M. L. Timmermans, D. K. Perovich, R. A. Krishfield, A. Proshutinsky, and J. Richter-Menge (2010), Influences of the ocean surface mixed layer and thermohaline stratification on Arctic Sea ice in the central Canada Basin, *J. Geophys. Res.*, *115*, C10018, doi:10.1029/2009JC005660.

United Nations Environment Programme (2013), Mercury—Time to Act, Oslo.

Vavrus, S., D. Waliser, A. Schweiger, and J. Francis (2009), Simulations of 20th and 21st century Arctic cloud amount in the global climate models assessed in the IPCC AR4, *Clim. Dyn.*, *33*, 1099–1115, doi:10.1007/s00382-008-0475-6.

Wang, F., R. W. Macdonald, D. A. Armstrong, and G. A. Stern (2012), Total and methylated mercury in the Beaufort Sea: The role of local and recent organic remineralization, *Environ. Sci. Technol.*, *46*, 11,821–11,828, doi:10.1021/es302882d.

Wilson, S., J. Munthe, K. Sundseth, K. Kindbom, P. Maxson, J. Pacyna, and F. Steenhuisen (2010), Updating historical global inventories of anthropogenic mercury emissions to air, 1–12 pp., Oslo.

Zhang, T. J., et al. (2005), Spatial and temporal variability in active layer thickness over the Russian Arctic drainage basin, *J. Geophys. Res.*, *110*, D16101, doi:10.1029/2004JD005642.